
Deep Convolutional Sum-Product Networks for Probabilistic Image Representations

Jos van de Wolfshaar^{1,2} Andrzej Pronobis^{1,3}

Abstract

Sum-Product Networks (SPNs) are hierarchical probabilistic graphical models capable of fast and exact inference. Applications of SPNs to real-world data such as large image datasets has been fairly limited in previous literature. We introduce Convolutional Sum-Product Networks (ConvSPNs) which exploit the inherent structure of images in a way similar to deep convolutional neural networks, optionally with weight sharing. ConvSPNs encode spatial relationships through local products and local sum operations. ConvSPNs obtain state-of-the-art results compared to other SPN-based approaches on several visual datasets, including color images, for both generative as well as discriminative tasks. ConvSPNs are the first pure-SPN models applied to color images that do not depend on additional techniques for feature extraction. In addition, we introduce two novel methods for regularizing SPNs trained with hard EM. Both regularization methods have been motivated by observing an exponentially decreasing variance of log probabilities with respect to the depth of randomly structured SPNs. We show that our regularization provides substantial further improvements in generative visual tasks.

1. Introduction

Sum-Product Networks (Poon & Domingos, 2011) are probabilistic graphical models (PGM) (Koller et al., 2009) designed with computational efficiency in mind. These networks allow for exact and efficient marginal, conditional and joint inference queries and naturally deal with missing data. Other PGMs like Markov Networks and Bayesian Networks are generally unable to compute *exact* inferences

in reasonable time for a large number of variables. SPNs can be seen as a special type of deep neural network that can be trained using the techniques commonly used in deep learning (Peharz et al., 2018), as well as other techniques used for PGMs (Zhao et al., 2016; Rashwan et al., 2018).

SPNs have been used for various visual tasks such as image completion (Poon & Domingos, 2011), classification (Poon & Domingos, 2011), classification with missing features (Jaini et al., 2018b; Peharz et al., 2018), novelty detection (Zheng et al., 2018) and more. However, SPNs have not yet excelled in domains with large amounts of high-dimensional data such as large image datasets. This work takes a first step towards enabling SPNs to successfully perform within these more challenging domains.

Computer vision has recently been dominated by convolutional neural networks (CNNs) (LeCun et al., 1990; Krizhevsky et al., 2012; Szegedy et al., 2015; He et al., 2015). CNNs share their weights across the spatial axes. Weight sharing reduces the risk of overfitting and, together with pooling operations, provides translation invariance. In addition, local connectivity ensures that features are learned locally and gradually increase in complexity when moving up the layer hierarchy. We explore similar architectures for SPNs which we refer to as Convolutional Sum-Product Networks (ConvSPNs). ConvSPNs exploit the inherent structure in image data by using local product and local sum operations, optionally with weight sharing. ConvSPNs yield generative and discriminative abilities for image data that substantially surpass SPN-based approaches from existing literature across several datasets.

Our main contributions are (i) the introduction of novel ConvSPN architectures (ii) an extensive range of experiments on image data with state-of-the-art performance among SPN models and (iii) the introduction of two new regularization methods for SPNs trained with hard EM. Both regularizations aim at alleviating the effect of an empirically validated relation between the depth of a randomly structured SPN with random weights and an exponentially decreasing variance of the log probability that causes hard EM to perform suboptimally. ConvSPNs are the first pure-SPN models applied to color images that do not depend on additional techniques for feature extraction.

¹Department of Robotics, Perception and Learning, KTH Royal Institute of Technology, Stockholm, Sweden ²MessageBird, Amsterdam, The Netherlands ³Paul G. Allen School of Computer Science & Engineering, University of Washington, Seattle, WA, USA. Correspondence to: Jos van de Wolfshaar <jos.vandewolfshaar@gmail.com>, Andrzej Pronobis <pronobis@cs.washington.edu>.

Our models leverage the efficiency of the modern computational TensorFlow framework (Abadi et al., 2015). Most of our code is part of a generic TensorFlow-based library¹ which enables joint, conditional, marginal and MPE inferences as well as generative and discriminative learning for SPNs (Pronobis et al., 2017). It also supports various input distributions so that it can handle both discrete and continuous data or a mix of both.

The paper is structured as follows: Section 2 discusses the theoretical background for SPNs. Section 3 discusses related research on SPN-based approaches for computer vision. Section 4 outlines our approach to ConvSPNs. In Section 5, we propose two novel methods for regularizing SPNs that are trained with hard EM. We then compare the performance of ConvSPNs to other SPNs from related literature for several image datasets in Section 6.

2. Background

A Sum-Product Network $S(\mathbf{x})$ represents a joint probability distribution over a set of random variables \mathbf{X} , where the individual variables X_i are discrete or continuous. An SPN is a rooted directed acyclic graph where the root node computes the unnormalized probability $S(\mathbf{x})$ of a distribution at $\mathbf{x} \in \mathbf{X}$. The leaf nodes correspond to individual random variables X_i . These variables can be either discrete or continuous. In the discrete case, they are typically represented as Bernoulli variables, while Gaussian distributions are often used in the continuous case. In between the leaf nodes and the root, the SPN contains weighted sums and product operations. The weighted sum nodes have non-negative weights and can be interpreted as defining a probabilistic mixture of their input nodes, while products compute joint probabilities of their inputs by multiplying their values. The output of a sum node is given by $s_j = \sum_{i \in \text{ch}(s_j)} w_{ji} C_i$ where C_i is the value of the i -th child and $\text{ch}(s_j)$ is the set of children of s_j . The output of a product node is given by $p_j = \prod_{i \in \text{ch}(p_j)} C_i$.

Following (Poon & Domingos, 2011), we define the following concepts related to SPNs:

Definition 1 (Scope). The scope of a node n , denoted $\text{sc}(n)$, is the set of variables that are descendants of n .

In other words, the scope of a node is the union of the scopes of its children. Leaf nodes have a *singular* scope containing a single variable X_i .

Definition 2 (Validity). An SPN is valid if it correctly computes the unnormalized probability for all evidence e where $e \subseteq \mathbf{X}$.

A sufficient set of conditions that ensure validity consists of *completeness* and *decomposability*:

Definition 3 (Completeness). An SPN is complete if all children of a sum node have identical scopes.

Definition 4 (Decomposability). An SPN is decomposable if all children of the same product node have pairwise disjoint scopes.

In other words, the scopes of the children of product nodes should have no variables in common.

Evaluating an SPN without any evidence gives the partition function $Z_S = \sum_{\mathbf{x} \in \mathbf{X}} S(\mathbf{x})$ which can be used as the normalization constant for computing the probability of \mathbf{x} : $P(\mathbf{x}) = S(\mathbf{x})/Z_S$. The constant Z_S is computed by setting the output of each leaf node to 1. For a Bernoulli variable X_i , both indicators X_i and \bar{X}_i are set to 1. If all X_i are continuous and represented as Gaussian leaf nodes, all of the Gaussian components corresponding to X_i are set to 1.

A *normalized* SPN contains *normalized sum nodes* of which the weights add up to one. It has been proven that $Z_{\bar{S}} = 1$ and thus $P(\mathbf{x}) = \bar{S}(\mathbf{x})$ where \bar{S} is a normalized SPN (Peharz, 2015). Hence, a valid normalized SPN accurately models a probability density function or a probability mass function. Hence, for some evidence $e \subseteq \mathbf{X}$, the probability $P(e)$ can be computed with a single forward pass in \bar{S} .

SPNs can be trained to perform both generative tasks (e.g. using hard EM) as well as discriminative tasks (e.g. using gradient descent).

3. Related Work

In this section we cover related work on computer vision with SPNs. In addition, we briefly elaborate on related work that covers weight sharing in SPNs.

3.1. Computer Vision With Sum-Product Networks

In (Peharz et al., 2018), SPNs with random decompositions, referred to as RAT-SPNs, are shown to yield performance on-par with multi-layer perceptrons (MLPs) on several image benchmarks, including the MNIST (Lecun et al., 1998) and Fashion MNIST (Xiao et al., 2017) datasets.

In (Rashwan et al., 2018), discriminative training of SPNs is accomplished through Extended Baum-Welch (EBW) instead of gradient descent methods. The SPN architecture used by (Rashwan et al., 2018) is constructed in a way similar to the image completion experiments in (Poon & Domingos, 2011), where each rectangular region is split into all possible vertical and horizontal rectangular subregions (APVAHRS). The smallest region in this APVAHRS architecture consists of a single pixel.

In (Hartmann, 2014), the authors feed the features of a CNN to an SPN and train the SPN discriminatively with SGD. This is the only related work that mentions convolutions

¹www.libspn.org

on images in the context of SPNs, but the convolutions themselves are not part of the SPN model.

In (Adel et al., 2015) SPNs are trained using an SVD-based structure learning algorithm which significantly outperformed other SPN learning algorithms at the time of publication. Another recent paper on structure learning for SPNs introduces the Prometheus algorithm (Jaini et al., 2018a). This paper also considers MNIST data and together with (Peharz et al., 2018) reports the best classification accuracy on the MNIST dataset thus far.

In (Poon & Domingos, 2011), image completion was performed on the Olivetti (Samaria & Harter, 1994) and Caltech (Fei-Fei et al., 2004) datasets showing superior results compared to other generative models.

Finally, (Gens & Domingos, 2012) introduce discriminative training for SPNs through gradient descent. For image classification on CIFAR-10 (Krizhevsky, 2009), they employ a patch-wise feature extraction method based on k-means and a ‘triangle’ encoding that is max-pooled and then followed by an SPN per class. At the time of publication they reported state-of-the-art accuracies on CIFAR-10.

3.2. Weight Sharing for Sum-Product Networks

Weight sharing for SPNs has been explored before in (Cheng et al., 2014) where the authors looked at language modeling. The weight sharing occurs in the very first layer of the network that is connected to one-hot word feature vectors. Hence, the first layer can be thought of as an embedding layer where the weights are constrained to be strictly positive. It is unclear to what extent the weight sharing improved the performance of the SPN based on the results discussed in (Cheng et al., 2014).

To summarize the above, previous work lacks an attempt to frame SPNs as convolutional architectures. Furthermore, the benefits of weight sharing in SPNs are not yet empirically assessed. We aim to cover both issues among others.

4. Convolutional Sum-Product Networks

We now present Convolutional SPNs (ConvSPNs), our new SPN architecture, which exploits the inherent structure of spatial data in a way similar to deep convolutional neural networks. Since our implementation is tensorized, we first explain the interpretation of each tensor dimension.

ConvSPNs consist of products or weighted sums that combine their inputs locally in a way similar to CNNs. As in most modern CNN layer implementations, ConvSPN layers are represented as 4D tensors with dimensions for (i) the samples in the batch (ii) the rows (iii) the columns and (iv) the channels. From hereon, we omit the batch dimension and discuss ConvSPNs for a single sample for simplicity.

We refer to all channels at a given location of a spatial tensor (e.g. $X[i, j, :]$) as a *cell*. A *node* corresponds to a single element of the spatial tensor, e.g. $X[i, j, k]$. Nodes are grouped in either spatial product layers or spatial sum layers.

An SPN must be *valid* to accurately model a joint probability distribution. As mentioned before, completeness and decomposability are sufficient properties to guarantee validity. We will now elaborate on how to guarantee both completeness in spatial sum layers and decomposability in spatial product layers. Then, we discuss how multiple convolutional layers are stacked to form a deep network.

4.1. Spatial Sum Layers

To maintain the *completeness* property of a sum node, it can only have child nodes with *identical scopes*. The input layer of a ConvSPN contains the image and consists of leaf distributions at different cells. Clearly, these cells are unique per pixel and so the first and second axis ($X[:, j, k]$ and $X[i, :, k]$ respectively) of the spatial tensor at the input can be thought of as scope axes. As a consequence, as soon as we consider different child cells ($X[i, j, :]$, $X[u, v, :]$, $i \neq u \vee j \neq v$), we cannot connect a sum node to children from both cells at the same time. Hence, sum nodes must be connected to cell regions of exactly 1×1 , so that a sum’s children correspond to all channels within a single cell. In our experiments, we consider spatial sum layers with shared weights (i.e. a 1×1 convolutional layer) as well as spatial sum layers without weight sharing.

4.2. Spatial Product Layers

To satisfy decomposability of product nodes, the scopes of a product’s children need to be *pairwise disjoint* (so $sc(C_i) \cap sc(C_j) = \emptyset, \forall i, j \in ch(p)$ s.t. $i \neq j$ where $ch(p)$ is the set of children of the product node). A spatial product layer combines the nodes of the preceding layer through local products of $k \times k$ patches. The scopes of these products form the union of the scopes under the current patch. In the non-log domain, local products cannot be framed as convolutions. For numerical stability, SPNs are implemented to propagate *log* probabilities. In the log-domain products become sums. Hence, local products can be implemented as convolutions in the log domain with unit weights. We refer to this interpretation as a *convolutional log-product* (CLP). The kernels of CLPs can be thought of as ‘one-hot’ in the sense that they have zeros in all but one channel per cell.

It is often infeasible to generate all possible permutations of product children in a CLP layer. For example, if there are 16 input channels and a patch size of 2×2 , then there are 16^4 possible combinations of product children per patch. To limit the number of products, one can take a random subset of combinations. A special case of a limited subset can

be obtained by computing *depth-wise* convolutions, so that the number of output channels equals the number of input channels (i.e. there is exactly one product per channel).

4.3. Stacking Layers

Stacking layers in a ConvSPN requires a careful design to preserve SPN validity. Spatial sums do not change the spatial layout of the scopes. However, CLPs combine patches of multiple *cells*, which consequently changes the spatial layout of the scopes. We propose two ways of building multi-layered ConvSPNs and elaborate on how to choose the strides, patch size and dilation rates for CLPs so that we ensure decomposability.

4.3.1. NON-OVERLAPPING CONVSPNS

The most straightforward ConvSPN architecture uses CLPs with strides as large as their kernel size. Let the input of a CLP be a tensor $I \in \mathbb{R}^{h_1 \times w_1 \times d_1}$ (height h_1 , width w_1 and depth d_1). The output of the layer is a tensor $O \in \mathbb{R}^{(h_1/h_F) \times (w_1/w_F) \times d_O}$ and its filter $F \in \mathbb{R}^{h_F \times w_F \times d_1 \times d_O}$. By using strides of $h_F \times w_F$, the neighboring patches *do not overlap*. As a result, the scopes in O at different cells are all disjoint and thus the ConvSPN is still decomposable at O . Equally sized strides and filters can be applied recursively. Whenever the spatial dimensions of the input to a CLP are not a multiple of the kernel size, we can pad accordingly by nodes with ‘no evidence’ and empty scopes, meaning that they always have probability one. This conveniently corresponds to *zero-padding* in the log domain.

4.3.2. WICKER CONVSPN

A more general architecture, which we call *wicker* ConvSPN, relies on a more complex spatial pattern of products. As opposed to non-overlapping ConvSPNs, wicker ConvSPNs allow for unit strides *without* the loss of decomposability. Figure 1 shows an example of a ConvSPN with a wicker pattern in 1D, where scopes are enumerated from 0 through 7. Although the kernel size remains 2 throughout all product layers in the architecture, we ensure decomposability by doubling the *dilation rate* (Yu & Koltun, 2016) at each CLP, starting at a dilation rate of 1. Note that (Yu & Koltun, 2016) also advocate the use of exponentially increasing dilations, albeit for convolutional neural networks, to circumvent the loss of feature resolution or coverage which would otherwise occur with strides larger than 1 or pooling layers. The maximum scope cardinality of each cell starts at 1 at the input and then increases to 2, 4 and 8 after applying the first, second and third product respectively. Due to padding, the actual scope cardinality might be smaller for cells that are near the spatial boundaries. Figure 1 also reflects the sparsity in the kernels of the log products as each product node only has one child per input channel.

Figure 1 illustrates an example of a *fully convolutional* SPN architecture. In practice, we can construct several arbitrary valid decompositions after any number of layers. We can further generalize the wicker ConvSPN architecture. First, we can use the same connectivity pattern with kernel sizes larger than two. In addition, striding can be used to reduce the number of decompositions. In the extreme case, the strides are as large as the kernel size so that there is exactly one decomposition (see Section 4.3.1). Figure 1 depicts the other extreme without any strides, resulting in eight decompositions. Finally, the wicker pattern also extends to a number of spatial dimensions larger than 2.

5. Regularization For Generative SPNs

Several regularization techniques have been proposed for SPNs. In (Poon & Domingos, 2011), L_0 regularization was used for training SPNs with hard EM. In (Peharz et al., 2018), dropout and input evidence masking was introduced for discriminative SPNs trained with gradient descent.

To further improve the performance of ConvSPNs, we introduce two regularization methods for SPNs trained with hard EM. Hard EM has proven to be an effective algorithm to train generative SPNs as it overcomes the vanishing gradient problem. Hard EM is accomplished by backpropagating the ‘hard’ gradients. Starting at the root node, we determine the path W_x , which is obtained by taking the maximum weighted child of a sum node, or by splitting the path for each product node to all of its children. For each sum node, the weights are determined by normalizing the path counts ℓ_{ji} (the number of times the weight was part of a path): $w_{ji} = \ell_{ji} / (\sum_k \ell_{jk})$. Although hard EM would formally require MPE inference in the forward pass, we follow the suggested modification in (Poon & Domingos, 2011) to use marginal inference in the forward pass instead.

Figure 2 displays how the variance of $\log(c_i)$ (where c_i is the probability of a sum child) decreases exponentially as we move from the leaf nodes to the root in a randomly structured SPN with random weights.² The variances attain extremely small values, suggesting that the (log) probability of sum inputs in the network converge to the same value as we move from leaf nodes to the root. Consequently, the value of the weights are *the only terms that matter* to select the maximum weighted sum input. In our preliminary experiments, we indeed observed that when randomly structured SPNs are trained with ‘vanilla’ online hard EM, the distribution of the weight counts for a single sum node tends to concentrate on a single weight with the other weights never being selected as the winner. As a result, the largest weight of the sum thereafter dominates the path selection.

²The figure was generated using binarized MNIST data and an SPN with 2 children per product and 4 mixtures for each group of products with the same scope.

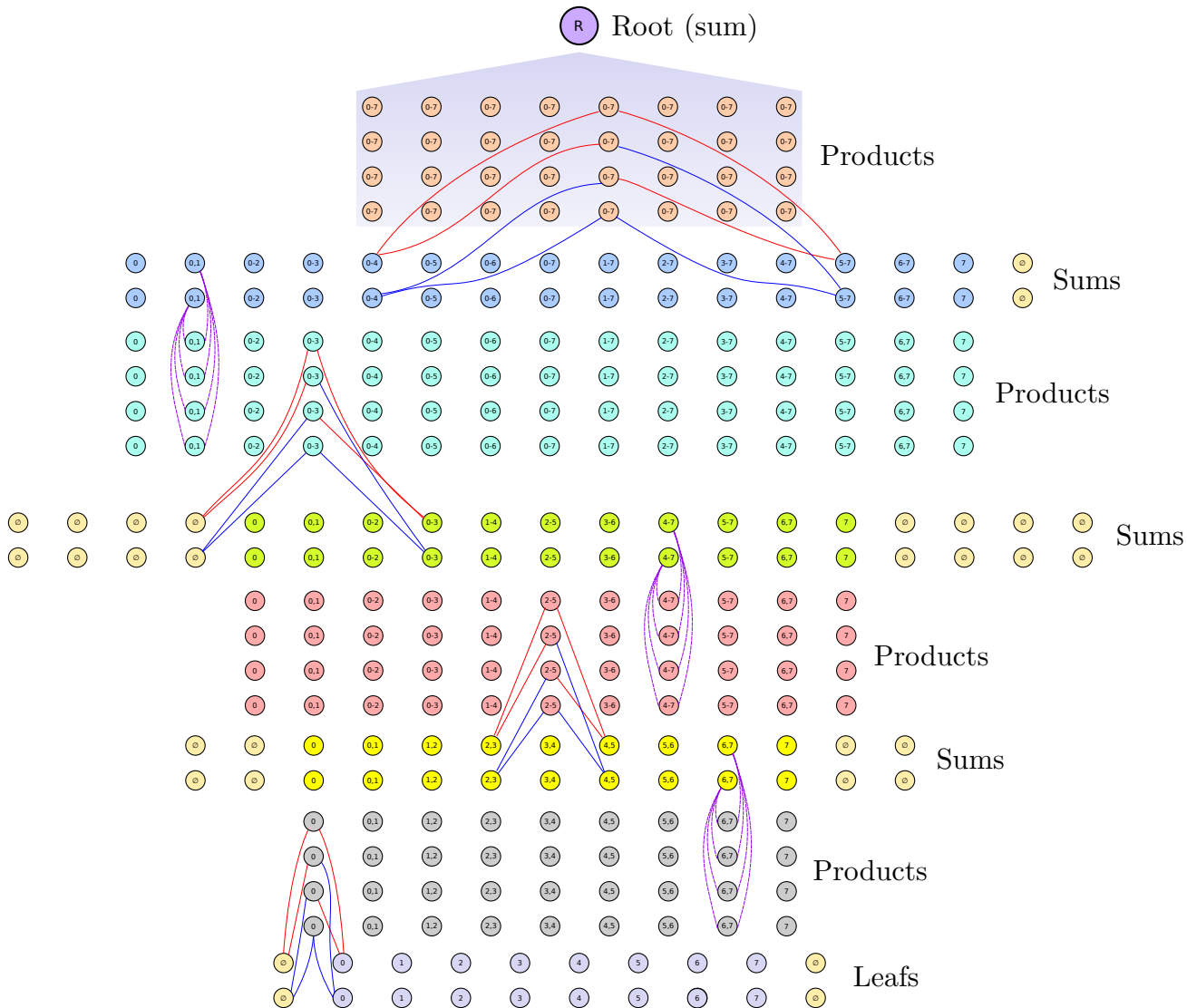


Figure 1. A simplified illustration of a wicker ConvSPN in 1D. Different layers are indicated by the color of the nodes. In each layer the nodes of a single cell (same column) share the same scope. The bottom layer contains the leaf distributions, where the row corresponds to the indicator (in case of discrete variables) or the distribution component (in case of continuous variables). Note that this SPN is fully convolutional (no fully connected layers) and that we effectively have 8 unique decompositions at the top. Every new layer of products doubles the dilation rate, starting at a rate of 1. Weighted sum layers are indicated by dashed purple connections. The connections are only drawn for a single cell per layer although the actual connections are repeated from left to right. The scopes of the nodes are indicated by the numbers within. Yellow padding nodes with empty scope sets are shown on the sides. Note that all nodes that are connected to the root node R have a scope of 0 through 7.

To alleviate the strong and immediate convergence to single weights in a sum node, we propose to either use *unweighted sum inputs in path selection* or *path selection by sampling*.

5.1. Unweighted Sum Inputs

To eliminate the effect of the sum weights on the path selection, we use the *unweighted* sum inputs to select the path. As a consequence, the weights of a sum node will never

enforce a single winning child on their own. We assess this regularization method in Section 6. Path selection by unweighted sum inputs has also been explored in another parameter learning algorithm in (Kalra et al., 2018). However, the experiments in (Kalra et al., 2018) do not assess the influence of this decision. In our experiments, we provide a comparison of unweighted vs. weighted sum children in path selection. We argue that the improved performance

is attributable to alleviating the problem of weights dominating path selection as a consequence of log probabilities converging to zero variance. Because of this convergence, it is important to break ties when selecting the winning child, which we accomplished by randomly sampling from the children with the maximum log probability.

5.2. MPE Path Sampling

Another way of alleviating the deterministic behavior of vanilla hard EM path selection is to sample the winning sum child with the probability given by normalizing the weighted probability of the sum child: $P(w_{ji} \in W_{\mathbf{x}}) = S_i(\mathbf{x})w_{ji} / (\sum_k S_k(\mathbf{x})w_{jk})$. In practice, we found that merely sampling does not necessarily yield optimal results. Therefore, we perform the sampling only with some probability p_{PS} and take the actual max child otherwise. Our experiments show the positive impact of this approach.

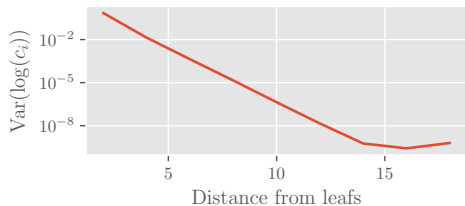


Figure 2. Average variance of $\log(c_i)$ (where c_i is the probability of the i -th child of a sum) for different layers in a sum-product network with random structure and random initial weights for MNIST data. The SPN used products with 2 children and 4 sums per scope. There appears to be an exponentially decreasing variance as the line is almost perfectly straight when viewed using log-scale, except for the values at a distance greater than 14. The latter is presumably caused by floating point precision errors.

6. Experiments

In this section we explore the discriminative and generative capabilities of ConvSPNs on visual tasks. As a generative task, we use image completion. We used image classification to evaluate our ConvSPNs on discriminative problems.

6.1. Learning and Hyperparameters

To train the generative SPNs, we use online hard EM (Poon & Domingos, 2011) with the regularization methods as proposed in Section 5. In addition, we use Gaussian leaf nodes of which the parameters are learned as proposed in (Kalra et al., 2018). We perform image completion by computing the marginal posterior probability at the Gaussian leaf distributions through partial derivatives (Darwiche, 2003). The partial derivatives are used as coefficients to linearly combine the modes of the leaf distributions, similar to (Poon

Table 1. Default hyperparameters. Both generative and discriminative settings are included. The table lists the number of channels for convolutional log-products (CLPs) and spatial sums (SS) for several image sizes n where the images have a shape of $n \times n$.

NAME	GENERATIVE / DISCRIMINATIVE
LEARNING ALGORITHM	HARD EM / AMSGRAD
LOG-SPACE WEIGHTS	FALSE / TRUE
KERNEL SIZE	2×2
DEPTH-WISE CLP	TRUE
# CH. SS $n \in \{28, 32\}$	[32, 64, 64, 128, 128]
# CH. SS $n = 64$	[32, 64, 64, 64, 128, 128]
# CH. SS $n = 100$	[32, 64, 64, 64, 64, 128, 128]
# CH. CLP $n \in \{28, 32\}$	[256, 32, 64, 64, 128, 128]
# CH. CLP $n = 64$	[256, 32, 64, 64, 64, 128, 128]
# CH. CLP $n = 100$	[256, 32, 64, 64, 64, 64, 128, 128]
STRIDES $n \in \{28, 32\}$	[1, 1, 1, 1, 1] / [2, 2, 1, 1, 1]
STRIDES $n = 64$	[1, 1, 1, 1, 1] / -
STRIDES $n = 100$	[1, 1, 1, 1, 1, 1] / -
LEAF DISTRIBUTION	NORMAL / CAUCHY
# COMPONENTS / PIXEL	4
LEAF SCALE	0.5, FIXED
LEAF LOCATION	EQUIDISTANT, TRAINABLE
DROPOUT p_{KEEP}	- / 0.9
INPUT MASK p_{KEEP}	- / 0.9
PATH SAMPLING p_{PS}	0.5 / -

& Domingos, 2011). The linear combinations form the actual predicted completion values. For discriminative SPNs, we use the AMSGrad optimizer (Reddi et al., 2018) to perform gradient descent as it proved to be more stable than the Adam optimizer (Kingma & Ba, 2014) in preliminary experiments across several datasets and learning rates. For discriminative SPNs, we only train the *location parameters* of either Gaussian or Cauchy leaf nodes. Color pixels are represented as a product of three univariate leafs corresponding to the red, green and blue channels. For all experiments, we performed sample-wise normalization by subtracting the mean and dividing by the standard deviation. We chose to use depth-wise convolutions as soon as the number of input channels exceeds 4. We generate all possible combinations of product children otherwise.

Several other SPN approaches, including those in (Gens & Domingos, 2012) or (Hartmann, 2014), require sub-SPNs *per class* after which the class-specific SPNs are combined by a single sum node at the root of the SPN. Consequently, these SPN architectures scale poorly when the number of classes is large. In contrast, our ConvSPNs achieve state-of-the-art results with only a single stack of product and sum layers which is shared for all classes followed by a layer of K sums (where K is the number of classes) and a root node. Hence, our ConvSPNs are scalable to datasets with potentially thousands of classes.

Whenever we apply dropout (Peharz et al., 2018), we do that throughout the entire network, except for the final sum node with the latent class indicator variable to avoid zero probability outputs.

Table 1 displays the default hyperparameter settings for our experiments. Since we employ a kernel size of 2×2 for all experiments, we generally require $\lceil \log_2(n) \rceil + 1$ CLPs for $n \times n$ images to join all scopes in the center as well as near the image boundaries (see also Figure 1), which corresponds to $2(\lceil \log_2(n) \rceil + 1)$ layers in total when including sum layers. Since our datasets vary in image sizes, we display the hyperparameters for different dimensions in Table 1.

6.2. Datasets

The MNIST dataset (Lecun et al., 1998) contains 60.000 28×28 gray-scale images of handwritten digits of which 55.000 are used for training and 5.000 are used for testing with 10 different classes. The Fashion MNIST (Xiao et al., 2017) dataset has the same number of images and image dimensions but contains images of pieces of cloth. The Olivetti dataset (Samaria & Harter, 1994) contains face images of 64×64 pixels. For the Caltech dataset (Fei-Fei et al., 2004) we use the same 100×100 crops as used in (Poon & Domingos, 2011). For Olivetti and Caltech we used the same train and test splits as used in (Poon & Domingos, 2011) to ensure a fair comparison. Finally, we used the CIFAR-10 dataset (Krizhevsky, 2009) with 55.000 train images and 5.000 test images of size 32×32 in color, again with 10 different classes.

Table 2. Unsupervised image completion. Regularization methods include L_0 , path sampling (PS), unweighted inputs (UI). The uppermost results for Olivetti and Caltech are taken from (Poon & Domingos, 2011). L_2 B corresponds to L_2 distance for the case when the bottom half of the image is masked and L_2 L is the corresponding distance where the left half is masked.

DATASET	REG.	ARCHITECTURE	L_2 B	L_2 L
OLIVETTI	L_0	APVAHRS	918	942
OLIVETTI	–	WICKERCONVSPN	917	879
OLIVETTI	UI	WICKERCONVSPN	859	875
OLIVETTI	PS	WICKERCONVSPN	799	756
OLIVETTI	PS, UI	WICKERCONVSPN	666	721
CALTECH	L_0	APVAHRS	3270	3551
CALTECH	PS	WICKERCONVSPN	2971	2979
CALTECH	PS	WICKERCONVSPN	2851	2971
CALTECH	UI	WICKERCONVSPN	2570	2529
CALTECH	PS, UI	WICKERCONVSPN	2504	2441
MNIST	PS, UI	WICKERCONVSPN	3058	2541
FMNIST	PS, UI	WICKERCONVSPN	1689	2215

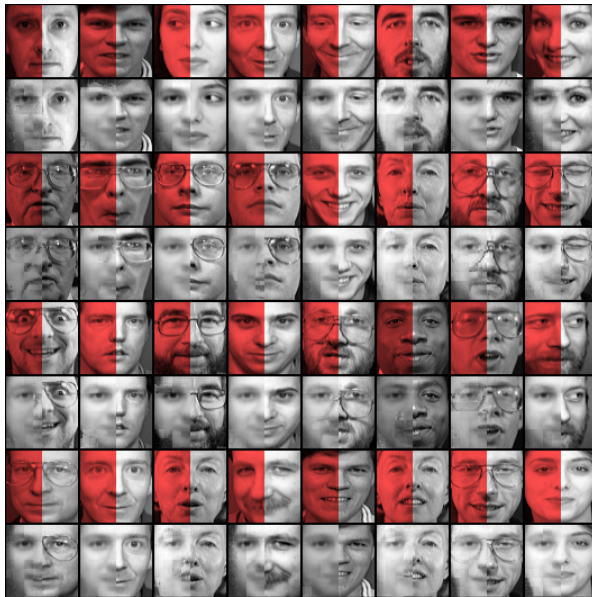


Figure 3. A random selection of completions for left-occluded test images from the Olivetti dataset. We alternate rows of original images (with masked part highlighted in red) and images with reconstructions done using wicker ConvSPNs. The average L_2 distance for this run was 713 (left) and 672 (right) which substantially outperforms (Poon & Domingos, 2011).

6.3. Results: Generative Learning

Table 2 shows the results for generative unsupervised learning. We task the model with a difficult problem of recreating half of an image based on its other half. We mask either the left or the bottom half of images in each dataset. The performance is assessed based on L_2 distance between the original data and the completions. We provide the average L_2 distance over the pixels scaled to the range of $[0, 255]$ on test data. Our ConvSPN models consistently outperform the SPNs in (Poon & Domingos, 2011). In addition, the table shows a clear gain in performance for our regularization approaches (MPE path sampling and using unweighted sum inputs) for both the Olivetti and Caltech datasets. Best performance is obtained for both types of regularization combined. This supports the suspicion that the decreasing variances of log probabilities are detrimental to the generative performance of SPNs trained with hard EM.

6.4. Results: Discriminative Learning

Table 3 provides an overview of our ConvSPN results together with the results from related work discussed in Section 3. For both MNIST and Fashion MNIST, we present results for a variety of configurations. In a subset of the experiments here, we augmented the data by taking random translations, rotations and crops.

Table 3. Results of discriminative experiments on multiple datasets for different regularizations: product dropout (PD), input dropout (ID), data augmentation (DA) and path sampling (PS) as well as weight sharing (WS). Models marked with * are pure-SPN approaches (the remaining approaches rely on an additional model for feature extraction).

DATA	ALGORITHM	ARCHITECTURE	LEAF DIST.	REG./SHARING	AUTHORS/NOTES	ACC.
MNIST	EBW	APVAHRS	BERNOULLI	NONE	(RASHWAN ET AL., 2018)*	95.07%
MNIST	DSPN-SVD	LEARNED	$\mathcal{N}(\mu, \sigma^2)$	NONE	(ADEL ET AL., 2015)*	97.34%
MNIST	PROMETHEUS	LEARNED	$\mathcal{N}(\mu, \sigma^2)$	NONE	(JAINI ET AL., 2018A)*	98.37%
MNIST	SGD	CNN + SPN	$\mathcal{N}(\mu, \sigma^2)$	NONE	(HARTMANN, 2014)	98.34%
MNIST	ADAM	RAT-SPN	$\mathcal{N}(\mu, \sigma^2 I)$	PD, ID	(PEHARZ ET AL., 2018)*	98.19%
MNIST	AMSGRAD	CONVSPN	$\mathcal{N}(\mu, \sigma^2)$	PD, ID	OURS*	98.43%
MNIST	AMSGRAD	CONVSPN	CAUCHY(x_0, γ)	PD, ID	OURS*	98.72%
MNIST	AMSGRAD	CONVSPN	CAUCHY(x_0, γ)	PD, DA, WS	OURS*	98.99%
MNIST	AMSGRAD	CONVSPN	CAUCHY(x_0, γ)	PD, DA	OURS*	99.19%
FMNIST	ADAM	RAT-SPN	$\mathcal{N}(\mu, \sigma^2 I)$	PD, ID	(PEHARZ ET AL., 2018)*	89.52%
FMNIST	AMSGRAD	CONVSPN	CAUCHY(x_0, γ)	PD, ID	OURS*	90.56%
FMNIST	AMSGRAD	CONVSPN	CAUCHY(x_0, γ)	PD, DA, WS	OURS*	90.58%
FMNIST	AMSGRAD	CONVSPN	CAUCHY(x_0, γ)	PD, DA	OURS*	91.63%
CIFAR-10	SGD	CNN + SPN	$\mathcal{N}(\mu, \sigma^2)$	NONE	(HARTMANN, 2014)	53.29%
CIFAR-10	AMSGRAD	CONVSPN	CAUCHY(x_0, γ)	PD, DA	OURS*	68.21%
CIFAR-10	SGD	K-MEANS + SPN	$\mathcal{N}(\mu, \sigma^2)$	NONE	(GENS & DOMINGOS, 2012)	83.76%

First of all, we see that all realizations of ConvSPNs outperform other SPN based approaches found in the literature for all but one dataset. Second, we can see that using Cauchy leafs leads to a considerable improvement over Gaussian leafs. The best results are obtained when combining dropout with data augmentation. Table 3 also shows results for using weight sharing (WS) in the first sum layer of the ConvSPN. Although the performance is slightly inferior compared to the ConvSPN architectures without weight sharing, it is still superior to all alternatives, while reducing the number of trainable parameters by 25 percent compared to architectures without weight sharing. Weight sharing is likely to result in improved accuracy for datasets with even more complex local features and a clear benefit of translation invariance. Lastly, we provided results for CIFAR-10 showing that ConvSPNs clearly outperform the combination of CNNs and SPNs from (Hartmann, 2014), while being inferior to (Gens & Domingos, 2012). However, our ConvSPNs are the only pure-SPN models for color images to date.

7. Discussion

This paper introduced Convolutional Sum-Product Networks (ConvSPNs) that bring SPNs closer to some of the best performing representations for complex visual data. We introduced two approaches to stack layers in a ConvSPN while preserving its validity. Wicker ConvSPNs are the most general form of valid ConvSPNs that allow for overlapping patches through exponentially increasing dilation rates. ConvSPNs outperform other SPN-based approaches for generative and discriminative tasks for image comple-

tion and classification. Moreover, ConvSPNs are the first pure-SPN models used for color images without additional feature extraction methods. As opposed to our ConvSPNs, alternative methods with additional feature extraction cannot be used for generative tasks such as image completion.

We introduced two regularization methods for hard EM which yield further improvements for generative tasks across several datasets. Further analysis on the phenomenon motivating our approaches is likely to provide a deeper understanding of generative learning techniques for SPNs.

As opposed to CNNs, ConvSPNs are probabilistic models which naturally deal with missing inputs and can be used for conditional, joint or marginal queries and can deal with both generative and discriminative tasks. However, ConvSPNs still show inferior classification performance compared to CNNs. We intend to further draw from the pool of ideas applied to CNNs and derive theoretical frameworks unifying the different approaches. Additionally, we continue investigating other types of leaf distributions (beyond Gaussian and Cauchy) for representing features in image data.

The proposed architecture is applicable to a wide range of spatial data beyond pure images and 2 dimensions. The ability to model such data probabilistically is extremely beneficial in certain domains such as robotics.

We hope to encourage further development and application of spatial SPN architectures by releasing the code as part of a general SPN learning library.³

³www.libspn.org

Acknowledgements

We would like to thank Avinash Raganath for his indispensable contributions to the LibSPN library and insightful discussions during the time we spent together at KTH.

This work was supported by the Swedish Research Council (VR) project 2012-4907 SKAEENet.

References

- Abadi, M., Agarwal, A., Barham, P., Brevdo, E., Chen, Z., Citro, C., Corrado, G. S., Davis, A., Dean, J., Devin, M., Ghemawat, S., Goodfellow, I., Harp, A., Irving, G., Isard, M., Jia, Y., Jozefowicz, R., Kaiser, L., Kudlur, M., Levenberg, J., Mané, D., Monga, R., Moore, S., Murray, D., Olah, C., Schuster, M., Shlens, J., Steiner, B., Sutskever, I., Talwar, K., Tucker, P., Vanhoucke, V., Vasudevan, V., Viégas, F., Vinyals, O., Warden, P., Wattenberg, M., Wicke, M., Yu, Y., and Zheng, X. TensorFlow: Large-scale machine learning on heterogeneous systems, 2015. URL <https://www.tensorflow.org/>. Software available from tensorflow.org.
- Adel, T., Balduzzi, D., and Ghodsi, A. Learning the structure of sum-product networks via an svd-based algorithm. In *Proceedings of the Thirty-First Conference on Uncertainty in Artificial Intelligence*, UAI'15, pp. 32–41, Arlington, Virginia, United States, 2015. AUAI Press. ISBN 978-0-9966431-0-8. URL <http://dl.acm.org/citation.cfm?id=3020847.3020852>.
- Cheng, W.-C., Kok, S., Pham, H. V., Chieu, H. L., and Chai, K. M. A. Language modeling with sum-product networks. In *INTERSPEECH*, 2014.
- Darwiche, A. A differential approach to inference in bayesian networks. *J. ACM*, 50(3):280–305, 2003. doi: 10.1145/765568.765570. URL <https://doi.org/10.1145/765568.765570>.
- Fei-Fei, L., Fergus, R., and Perona, P. Learning generative visual models from few training examples: An incremental bayesian approach tested on 101 object categories. In *2004 Conference on Computer Vision and Pattern Recognition Workshop*, pp. 178–178, June 2004. doi: 10.1109/CVPR.2004.383.
- Gens, R. and Domingos, P. Discriminative learning of sum-product networks. In Pereira, F., Burges, C. J. C., Bottou, L., and Weinberger, K. Q. (eds.), *Advances in Neural Information Processing Systems 25*, pp. 3239–3247. Curran Associates, Inc., 2012.
- Hartmann, T. *Discriminative Convolutional Sum-Product Networks on GPU*. PhD thesis, Rheinische Friedrich-Wilhelms-Universität Bonn, 2014.
- He, K., Zhang, X., Ren, S., and Sun, J. Deep residual learning for image recognition. *CoRR*, abs/1512.03385, 2015. URL <http://arxiv.org/abs/1512.03385>.
- Jaini, P., Ghose, A., and Poupart, P. Prometheus : Directly learning acyclic directed graph structures for sum-product networks. In Kratochvíl, V. and Studený, M. (eds.), *Proceedings of the Ninth International Conference on Probabilistic Graphical Models*, volume 72 of *Proceedings of Machine Learning Research*, pp. 181–192, Prague, Czech Republic, 11–14 Sep 2018a. PMLR. URL <http://proceedings.mlr.press/v72/jaini18a.html>.
- Jaini, P., Poupart, P., and Yu, Y. Deep homogeneous mixture models: Representation, separation, and approximation. In Bengio, S., Wallach, H., Larochelle, H., Grauman, K., Cesa-Bianchi, N., and Garnett, R. (eds.), *Advances in Neural Information Processing Systems 31*, pp. 7136–7145. Curran Associates, Inc., 2018b.
- Kalra, A., Rashwan, A., Hsu, W.-S., Poupart, P., Doshi, P., and Trimonias, G. Online structure learning for feed-forward and recurrent sum-product networks. In Bengio, S., Wallach, H., Larochelle, H., Grauman, K., Cesa-Bianchi, N., and Garnett, R. (eds.), *Advances in Neural Information Processing Systems 31*, pp. 6944–6954. Curran Associates, Inc., 2018.
- Kingma, D. P. and Ba, J. Adam: A method for stochastic optimization. *CoRR*, abs/1412.6980, 2014.
- Koller, D., Friedman, N., and Bach, F. *Probabilistic graphical models: principles and techniques*. MIT press, 2009.
- Krizhevsky, A. Learning multiple layers of features from tiny images. Technical report, 2009.
- Krizhevsky, A., Sutskever, I., and Hinton, G. E. Imagenet classification with deep convolutional neural networks. In *Proceedings of the 25th International Conference on Neural Information Processing Systems - Volume 1*, NIPS'12, pp. 1097–1105, USA, 2012. Curran Associates Inc. URL <http://dl.acm.org/citation.cfm?id=2999134.2999257>.
- LeCun, Y., Boser, B., Denker, J. S., Henderson, D., Howard, R. E., Hubbard, W., and Jackel, L. D. Handwritten digit recognition with a back-propagation network. In Touretzky, D. (ed.), *Advances in Neural Information Processing Systems (NIPS 1989)*, volume 2, Denver, CO, 1990. Morgan Kaufman.
- Lecun, Y., Bottou, L., Bengio, Y., and Haffner, P. Gradient-based learning applied to document recognition. In *Proceedings of the IEEE*, pp. 2278–2324, 1998.

- Peharz, R. *Foundations of sum-product networks for probabilistic modeling*. PhD thesis, Graz University of Technology, 2015.
- Peharz, R., Vergari, A., Stelzner, K., Molina, A., Trapp, M., Kersting, K., and Ghahramani, Z. Probabilistic deep learning using random sum-product networks. *arXiv preprint arXiv:1806.01910*, 2018.
- Poon, H. and Domingos, P. Sum-product networks: A new deep architecture. In *Computer Vision Workshops (ICCV Workshops), 2011 IEEE International Conference on*, pp. 689–690. IEEE, 2011.
- Pronobis, A., Ranganath, A., and Rao, R. P. LibSPN: A library for learning and inference with Sum-Product Networks and TensorFlow. In *ICML 2017 Workshop on Principled Approaches to Deep Learning*, Sydney, Australia, August 2017. URL <http://www.libspn.org>.
- Rashwan, A., Poupart, P., and Zhitang, C. Discriminative training of sum-product networks by extended baum-welch. In Kratochvíl, V. and Studený, M. (eds.), *Proceedings of the Ninth International Conference on Probabilistic Graphical Models*, volume 72 of *Proceedings of Machine Learning Research*, pp. 356–367, Prague, Czech Republic, 11–14 Sep 2018. PMLR. URL <http://proceedings.mlr.press/v72/rashwan18a.html>.
- Reddi, S. J., Kale, S., and Kumar, S. On the convergence of adam and beyond. In *International Conference on Learning Representations*, 2018. URL <https://openreview.net/forum?id=ryQu7f-RZ>.
- Samaria, F. S. and Harter, A. C. Parameterisation of a stochastic model for human face identification. In *Proceedings of 1994 IEEE Workshop on Applications of Computer Vision*, pp. 138–142, Dec 1994. doi: 10.1109/ACV.1994.341300.
- Szegedy, C., Liu, W., Jia, Y., Sermanet, P., Reed, S., Anguelov, D., Erhan, D., Vanhoucke, V., and Rabinovich, A. Going deeper with convolutions. In *The IEEE Conference on Computer Vision and Pattern Recognition (CVPR)*, June 2015.
- Xiao, H., Rasul, K., and Vollgraf, R. Fashion-mnist: a novel image dataset for benchmarking machine learning algorithms, 2017.
- Yu, F. and Koltun, V. Multi-scale context aggregation by dilated convolutions. In *ICLR*, 2016.
- Zhao, H., Poupart, P., and Gordon, G. J. A unified approach for learning the parameters of sum-product networks. In Lee, D. D., Sugiyama, M., Luxburg, U. V., Guyon, I., and Garnett, R. (eds.), *Advances in Neural Information Processing Systems 29*, pp. 433–441. Curran Associates, Inc., 2016.
- Zheng, K., Pronobis, A., and Rao, R. P. N. Learning graph-structured sum-product networks for probabilistic semantic maps. In *Proceedings of the Thirty-Second AAAI Conference on Artificial Intelligence, (AAAI-18), the 30th innovative Applications of Artificial Intelligence (IAAI-18), and the 8th AAAI Symposium on Educational Advances in Artificial Intelligence (EAAI-18), New Orleans, Louisiana, USA, February 2-7, 2018*, pp. 4547–4555, 2018. URL <https://www.aaai.org/ocs/index.php/AAAI/AAAI18/paper/view/16923>.